Earth Planets Space, **56**, 239–248, 2004

Three-dimensional inversion of static-shifted magnetotelluric data

Yutaka Sasaki

Department of Earth Resources Engineering, Kyushu University, Hakozaki, Higashi-ku, Fukuoka 812-8581, Japan

(Received September 3, 2003; Revised February 18, 2004; Accepted February 23, 2004)

A practical method for inverting static-shifted magnetotelluric (MT) data to produce a 3-D resistivity model is presented. Static-shift parameters are incorporated into an iterative, linearized inversion method, with a constraint added on the assumption that static shifts are due to a zero-mean, Gaussian process. A staggered finite-difference scheme is used to evaluate both the forward problem and the 'pseudo-forward' problem needed to construct the full sensitivity matrix. The linear system of equations is efficiently solved by alternating the incomplete Cholesky biconjugate gradient (ICBCG) solver with the static divergence correction procedure. Even with this efficiency in the forward modeling, generating the full sensitivity matrix at every iteration is still impractical on modern PCs. To reduce the computer time to a reasonable level, an efficient procedure for updating the sensitivities is implemented: (1) in the first few iterations, the sensitivities for the starting homogeneous half-space are used, (2) the full sensitivity matrix is computed only once (e.g. at the third iteration), and (3) for the subsequent iterations it is updated using Broyden's algorithm. The synthetic and real data examples show that the method is robust in the presence of static shifts and can be used for 3-D problems of realistic size.

Key words: Magnetotellurics, 3-D inversion, static shift, Gauss-Newton method.

1. Introduction

Considerable advances have been made over the last decade in the 3-D inversion of magnetotelluric (MT) data. Mackie and Madden (1993) present an efficient algorithm that solves the least-squares inverse problem using the conjugate gradient method. Newman and Alumbaugh (2000) implement a non-linear conjugate gradient method to avoid excessive evaluations of the forward problem. Zhdanov *et al*. (2000) develop a rapid 3-D inversion algorithm based on their quasi-linear approximation of the forward modeling. Yamane *et al*. (2000) extend their 'generalized rapid relaxation inversion' (GRRI) scheme to the 3-D problem, which originated from the RRI of Smith and Booker (1991). All these methods share a common strategy in the sense that the calculation of the full sensitivity matrix is avoided. In the context of this issue, Rodi and Mackie (2001) predict, based on comparisons of 2-D inversion algorithms, that the standard Gauss-Newton algorithms will not be practical for realistic 3-D problems in favour of the conjugate gradient-based algorithms, while Siripunvaraporn and Egbert (2000) argue that their data-subspace inversion method, which belongs to the Gauss-Newton type approach, can be practically efficient for 3D problems.

One important issue that has not been addressed in the previous work is the removal of static shift. The effect of static shift is due to the presence of small-scale near-surface inhomogeneities, and manifests itself as a vertical shifting of the apparent resistivity curve by a frequency-independent factor, without any corresponding change in the phase curve. The amount of static shift varies from site to site, and differs depending on the source polarization. Thus, the interpretation of static-shifted MT data will obviously lead to erroneous results unless static shifts are correctly taken into account. One possible approach to counter static shifts in 3-D inversion might be to make the model parameterization fine enough to let the inversion compensate for static shifts by incorporating near-surface structure. However, this increases considerably the computation required for the forward modeling. Besides, there remains a question on how the near-surface structure obtained, which is highly likely to be erroneous, affects the reconstruction of larger-scale structure of interest. The model parameterization should be produced in view of the data collection parameters, such as the site spacing and the frequency range.

This paper describes a 3-D inversion method that solves simultaneously for both resistivities and static shift parameters, as is done in 2-D inversions by deGroot-Hedlin (1991) and Ogawa and Uchida (1996). The method uses a typical Gauss-Newton approach that requires the generation of the sensitivity matrix, with modifications made to reduce the number of forward-modeling applications to a reasonable level. The forward modeling is based on an efficient staggered-grid finite-difference technique. The inversion method is tested on a synthetic data set and a real data set from a geothermal field.

2. Inversion Method

Static shifts are manifested as vertical displacements of apparent resistivity curves when plotted on a log-coordinate scale; i.e.

$$\ln \rho_a^d = \ln \rho_a^u + s, \tag{1}$$

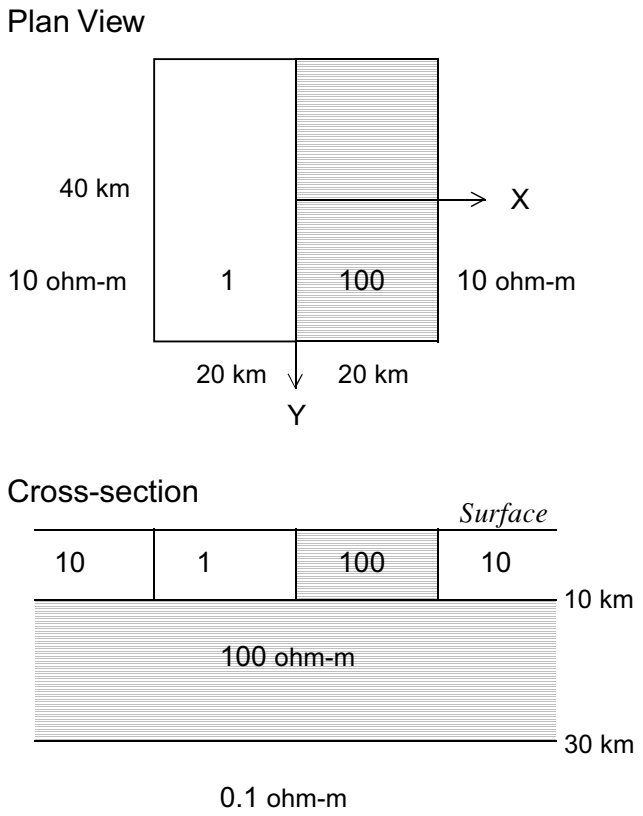

Fig. 1. 3-D model used to compare the finite-difference modelling results with the sampling schemes of types 1 and 2.

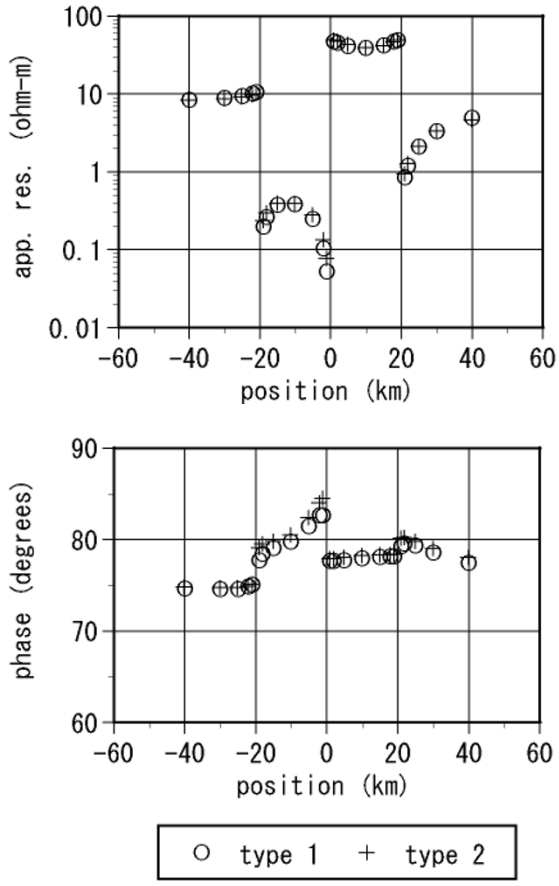

Fig. 2. Comparisons of the apparent resistivities and phases for the xy mode at a period of 1000 s, calculated from the staggered-grid finite-difference solutions with the sampling schemes of types 1 (circle) and 2 (cross).

where ρ_a^d is the distorted apparent resistivity, ρ_a^u is the undistorted apparent resistivity, and s is a static shift value. Thus, the MT inverse problem can be written in matrix form as

$$\mathbf{d} \cong \mathbf{F}(\mathbf{m}) + \mathbf{G}\mathbf{s}, \tag{2}$$

where $\mathbf{d}$ is a vector of the observed data that are composed of the natural logarithms of apparent resistivities and the phases, $\mathbf{F}(\mathbf{m})$ is the forward modeling function that generates the (undistorted) responses for the discretized model $\mathbf{m}$, and $\mathbf{G}$ is a matrix that relates the unknown static shift parameters $\mathbf{s}$ to the data $\mathbf{d}$. Note that $\mathbf{s}$ is linearly related to $\mathbf{d}$. The rows of $\mathbf{G}$ corresponding to the phases, which are independent of $\mathbf{s}$, are zeroes, and the rows corresponding to the apparent resistivities have one at the appropriate locations.

Because the inverse problem is non-linear in $\mathbf{m}$, it is iteratively solved for updated values of $\mathbf{m}$ (e.g., Tarantola, 1987). Let $\mathbf{m}^{(k)}$ be the model at the k-th iteration. Equation (2) can be linearized about $\mathbf{m}^{(k)}$ as

$$\Delta\mathbf{d} \cong \mathbf{A}\,\Delta\mathbf{m}^{(k)} + \mathbf{G}\mathbf{s}, \tag{3}$$

where $\mathbf{A}$ is the sensitivity matrix (or the matrix of first-order derivatives of F with respect to the model parameters), $\Delta\mathbf{m}^{(k)}$ is the perturbation from the current model, and

$$\Delta\mathbf{d} = \mathbf{d} - \mathbf{F}(\mathbf{m}^{(k)}) \tag{4}$$

is the vector of differences between the observed and predicted data. The least-squares solution of Eq. (3) is numerically unstable in the presence of noise. Therefore the solution should be restricted based upon available a priori information. This can be accomplished by defining an objective function,

$$U = \left\|\mathbf{W}\left[\Delta\mathbf{d} - \mathbf{A}\Delta\mathbf{m}^{(k)} - \mathbf{G}\mathbf{s}\right]\right\|^2 + \lambda^2 \cdot \left(\left\|\mathbf{C}\left(\mathbf{m}^{(k)} + \Delta\mathbf{m}^{(k)}\right)\right\|^2 + \alpha^2\left\|\Delta\mathbf{m}^{(k)}\right\|^2\right) + \beta^2\|\mathbf{s}\|^2, \tag{5}$$

where $\mathbf{W}$ is a diagonal matrix assigning weights to each datum according to its standard deviation, $\mathbf{C}$ is a second-difference (Laplacian) operator used to quantify the model roughness, and $\|\cdot\|^2$ represents the l_2 norm. The first term on the right-hand side of Eq. (5) represents data misfit. The second term is the constraint term acting on the model that includes the smoothness constraint and the one that limits the 'size' of $\Delta\mathbf{m}^{(k)}$ (Marquardt, 1963). The last term is added to impose a constraint on the static shifts on the assumption that they are Gaussian distributed with a mean of zero (Ogawa and Uchida, 1996). The parameter λ is a Lagrange multiplier or regularization parameter, and α and β are adjustable constants.

The minimization of U is equivalent to solving the aug-

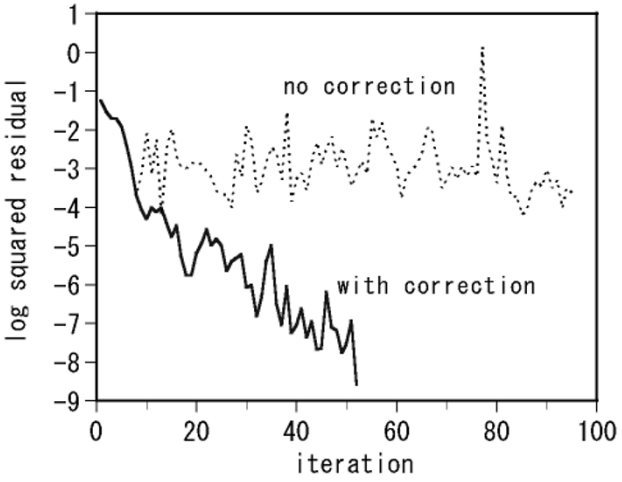

Fig. 3. Plot of the squared residual versus iteration number for the calculation of Fig. 2 using the ICBCG method with and without the static divergence corrections.

mented system

$$\begin{bmatrix} \mathbf{WA} & \mathbf{WG} \\ \lambda\mathbf{C} & 0 \\ \lambda\alpha\mathbf{I} & 0 \\ 0 & \beta\mathbf{I} \end{bmatrix} \begin{Bmatrix} \Delta\mathbf{m}^{(k)} \\ \mathbf{s} \end{Bmatrix} = \begin{Bmatrix} \mathbf{W}\Delta\mathbf{d} \\ -\lambda\mathbf{C}\mathbf{m}^{(k)} \\ 0 \\ 0 \end{Bmatrix}, \tag{6}$$

where $\mathbf{I}$ is the identity matrix. In this study, the modified Gram-Schmidt method is used to solve Eq. (6). The vector $\Delta\mathbf{m}^{(k)}$ is added to the current model $\mathbf{m}^{(k)}$ to give the new model. The iteration is continued until the data misfit measure is reduced to an acceptable level. The *rms* data error used in this study is given by

$$R = \sqrt{\frac{\sum_{i=1}^{N/2} \left\{ \left[\ln\left(\rho_{ai}^{o}/\rho_{ai}^{p}\right) \right]^2 + w^2 \left(\phi_i^o - \phi_i^p\right)^2 \right\}}{N}}, \tag{7}$$

where ρ_{ai} is the apparent resistivity, ϕ_i is the phase in degrees, the superscripts o and p refer to observed and predicted, respectively, and N is the number of data points. The value of w represents the weight assigned to the phase relative to the apparent resistivity and is set to 0.1. Equation (7) can be used as a misfit measure if the data are assumed to have the same standard deviations.

In solving Eq. (6), the value of λ must be determined so that an acceptable data misfit is achieved. This requires some form of trial and error. At each iteration, Equation (6) is solved using several trial values of λ, and for each updated model, forward modeling is carried out to calculate the data misfit R. By approximating the relationship between R and λ by a polynomial, a new value of λ that will minimize the misfit is estimated. In this study, four forward modelings are performed at each iteration to find λ. The value of α is fixed at 0.2. The choice of β that relates to the size of static shifts will be discussed later.

3. Forward Modeling

The forward solution for the 3-D electromagnetic fields can be formulated with Maxwell's differential equation for

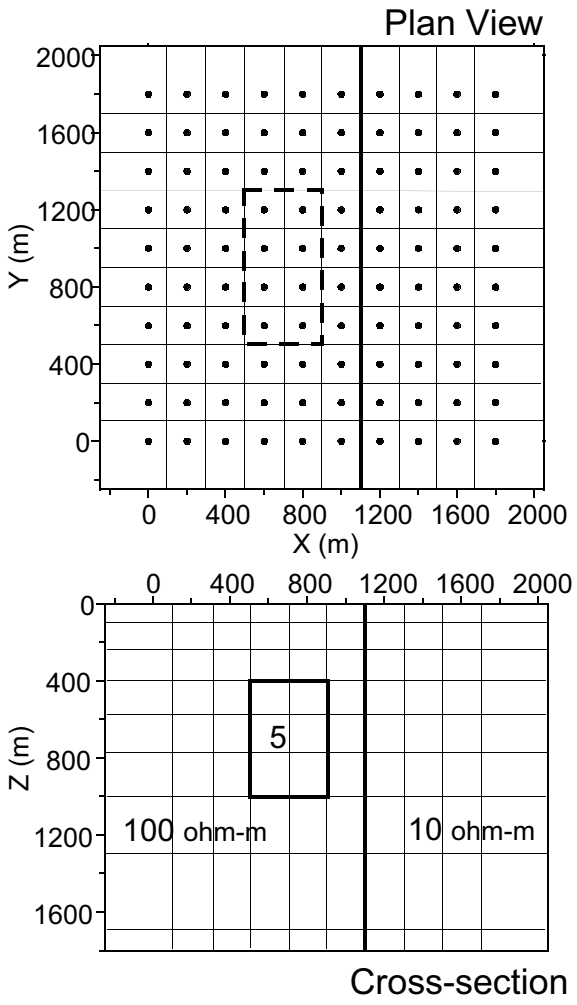

Fig. 4. 3-D model used to generate the synthetic data set. The 100 site locations are indicated by the closed circles. The block discretization is also shown.

the electric field in the frequency domain. If displacement currents are negligible and an $e^{i\omega t}$ time-dependence is assumed, then for plane-wave excitation the electric field, $\mathbf{E}$, satisfies the second-order differential equation

$$\nabla \times \nabla \times \mathbf{E} + i\omega\mu_0\sigma\mathbf{E} = 0, \tag{8}$$

where σ is the conductivity, μ_0 is the magnetic permeability of free space, ω is the angular frequency, and $i = \sqrt{-1}$.

As will be mentioned later, constructing the sensitivity matrix requires the forward solution of the electric fields due to finite sources such as an electric dipole. For excitation by a finite source, to avoid the singularity at the source, the total field is separated into the primary part $\mathbf{E}_p$ and the secondary part $\mathbf{E}_s$; i.e.

$$\mathbf{E} = \mathbf{E}_p + \mathbf{E}_s. \tag{9}$$

Then, the equation to be solved can be written as

$$\nabla \times \nabla \times \mathbf{E}_s + i\omega\mu_0\sigma\mathbf{E}_s = -i\omega\mu_0(\sigma - \sigma_p)\mathbf{E}_p, \tag{10}$$

where σ_p is the background conductivity (either a uniform or layered half-space). Once the electric field is determined, the magnetic field can be obtained through

$$\mathbf{H} = -\frac{1}{i\omega\mu_0}\nabla \times \mathbf{E}. \tag{11}$$

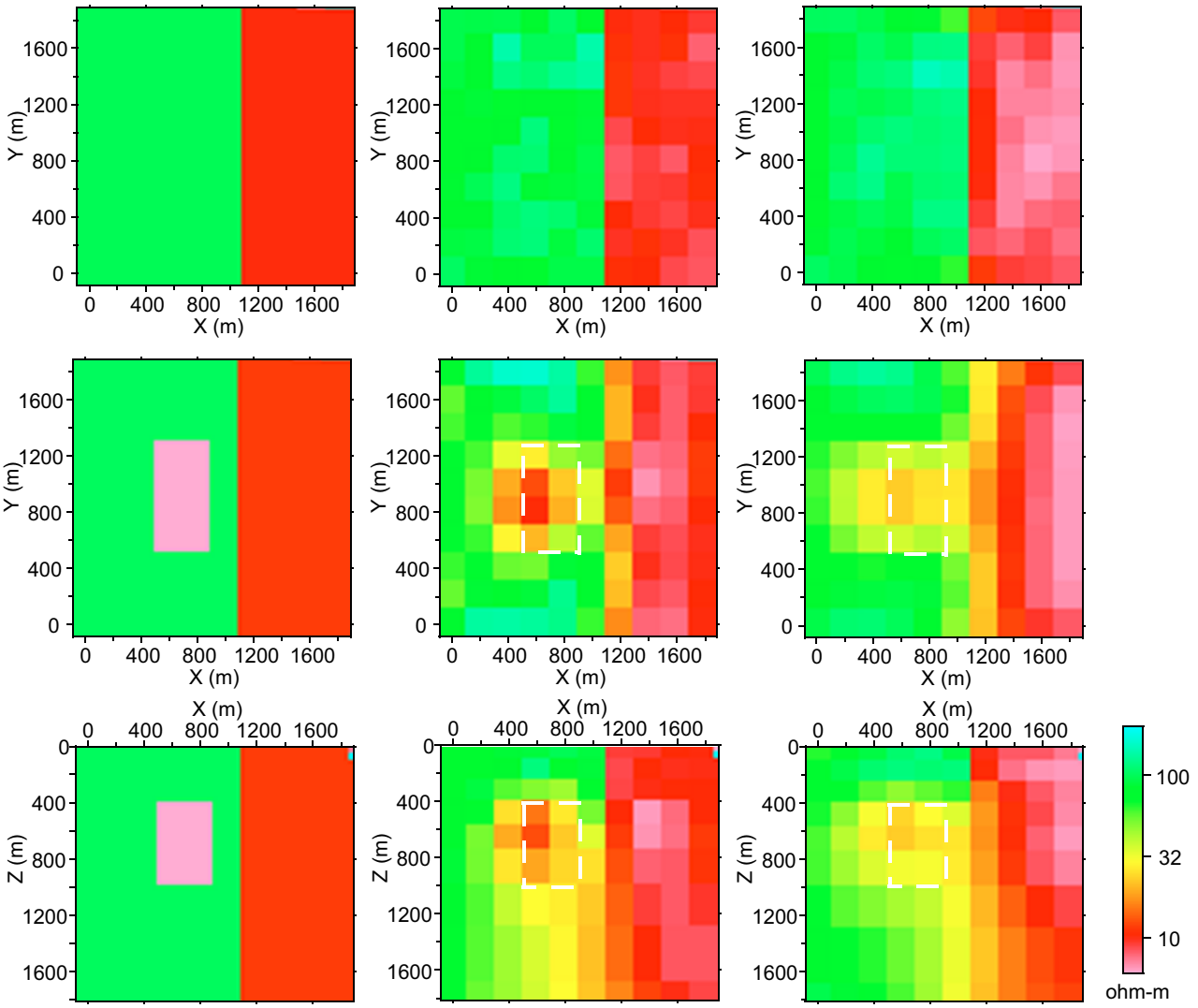

Fig. 5. Different horizontal and vertical sections for the true model and corresponding inversion models. The true model is shown in the first column, and the inversion models obtained with and without the update procedure are shown in the second and third columns, respectively. The top and second rows show the horizontal sections for depths of 150 and 700 m, respectively. The bottom row shows the vertical section for $y = 1000$ m. The position of the true 3-D body is outlined by the white dashed lines in the inversion models.

For a finite difference scheme on a staggered grid, the electric fields can be sampled at the centre of either the cell edges (Newman and Alumbaugh, 1995) or cell faces (Smith, 1996a). Hereafter, the two types of sampling schemes are referred to as 'type 1' and 'type 2', and both will be examined for accuracy. The conductivity at the sampling positions of type 1 is represented by a value averaged over the four adjoining cells, while the conductivity for type 2 is the inverse of the average resistivity of the two adjacent cells. As boundary conditions, the tangential component of the sampled field on the grid boundary is specified depending on the source polarization for the plane wave problem, and is set to zero for the finite source problem. Approximating Eq. (8) or (10) with finite difference results in a linear system of equations

$$\mathbf{Kf} = \mathbf{s}, \tag{12}$$

where $\mathbf{K}$ is a complex symmetric matrix, $\mathbf{f}$ is the unknown vector of the electric fields, and $\mathbf{s}$ is the vector that depends on the source term and the boundary conditions.

Equation (12) can be solved using the biconjugate gradient (BCG) method, preconditioned with an incomplete Cholesky decomposition. The preconditioning schemes using standard incomplete Cholesky decompositions break down because $\mathbf{K}$ is not positive-definite. However, Mackie *et al.* (1994) show that this difficulty can be avoided by applying the decomposition to only the diagonal subblocks that are positive-definite when $\mathbf{K}$ is grouped into subblocks depending on the related components of the electric fields. Although in many instances reasonable convergence rates can be obtained with the incomplete Cholesky biconjugate gradient (ICBCG) method, they tend to degrade at lower frequencies. This is because conservation of current is not guaranteed in a discretized version of Eq. (8) or (10) when the second term of the left-hand side is small. Smith (1996b) derived a correction procedure that enforces divergence-free conditions on the current density in the earth and the electric field in the air. The convergence rate can be improved significantly by alternating ICBCG iterations with this correction procedure.

The finite-difference modeling outlined above is tested on the model shown in Fig. 1. This model is used in Mackie

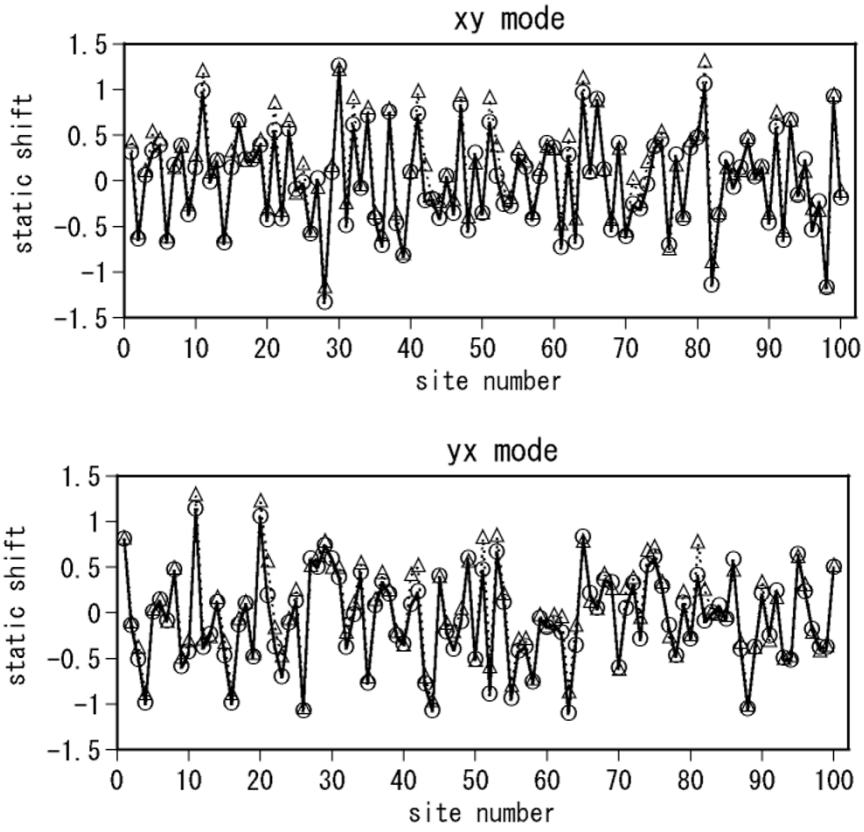

Fig. 6. Static shifts included in the synthetic data set (circles) and corresponding static shifts recovered by inversion (triangles). The top panel is for the xy mode and the bottom is for the yx mode.

et al. (1993) to compare the accuracy and efficiency of integral equation and finite difference results. Figure 2 shows the comparison of two different solutions for the xy mode response at a period of 1000 s along the x-axis. In this figure, the open circles and crosses show the results computed on a $29 \times 21 \times 22$ grid using the sampling schemes of types 1 and 2, respectively. The agreement is good in both the apparent resistivities and the phases. Since there is very little difference in both accuracy and efficiency between types 1 and 2, only the solution with type 1 is used hereafter. In Fig. 3, the squared residual is plotted as a function of iteration number for the cases with and without divergence corrections. With corrections, the relative residual is reduced to 10^{-8} after 52 iterations. This computation (one frequency and two source polarizations) took about 6 seconds on a 2.53-GHz Pentium 4 PC.

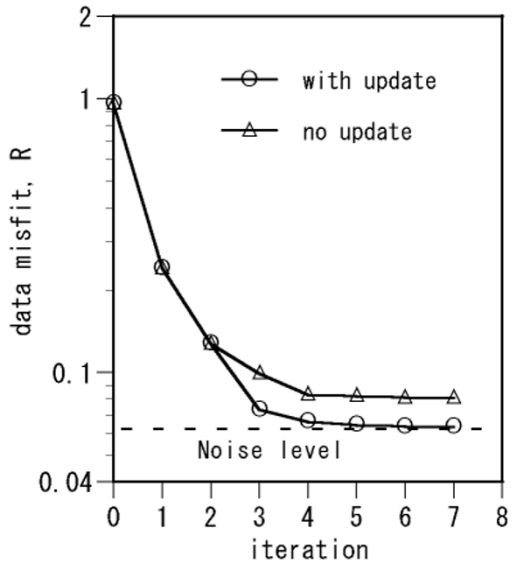

Fig. 7. Plot of *rms* data misfit versus iteration number for the inversions resulting in the models shown in Fig. 5.

4. Sensitivities

The sensitivities of the MT response are derived from those of the electric and magnetic field components at the surface. The sensitivities of these fields with respect to the conductivity of a block, σ_k, can be obtained from the forward modeling results by the adjoint-equation method (Weidelt, 1975; Mackie and Madden, 1993; McGillivray *et al*., 1994, among others). For example, the sensitivity for the x-component of the electric field can be written as

$$\frac{\partial E_x}{\partial \sigma_k} = \int \tilde{\mathbf{E}} \cdot \mathbf{E}\, dv, \tag{13}$$

where $\tilde{\mathbf{E}}$ is the electric field in the block due to an x-directed unit electric dipole at the receiving location, and $\mathbf{E}$ is the electric field due to the plane-wave source. The sensitivity of the magnetic field is given similarly to Eq. (13) as

$$\frac{\partial H_y}{\partial \sigma_k} = -\frac{1}{i\omega\mu} \int \tilde{\mathbf{E}} \cdot \mathbf{E}\, dv. \tag{14}$$

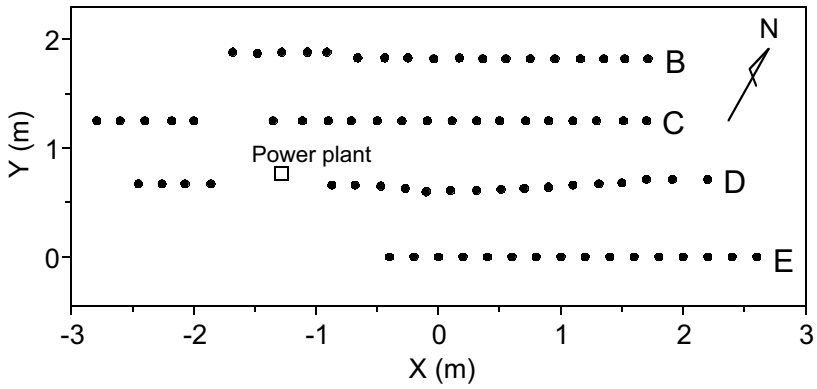

Fig. 8. Locations of the MT sites in the Kakkonda geothermal field. The approximate location of the geothermal power plant is also shown.

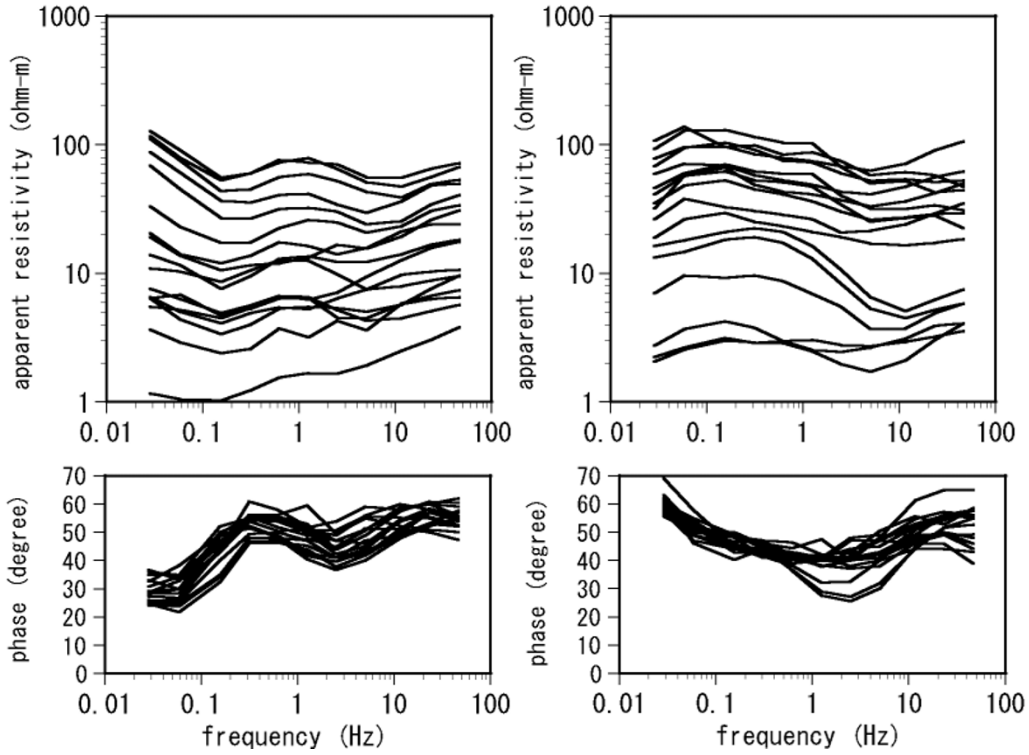

Fig. 9. Apparent resistivity (top) and phase curves (bottom) from all 18 locations along line B. The left panels are for the xy mode, and the right panels are for the yx mode.

Here, $\tilde{\mathbf{E}}$ is now defined as the electric field due to a y-directed magnetic dipole with unit moment at the receiving location. One can compute the sensitivities for any field components by doing an additional forward modeling for an appropriate finite source at the measurement site and by integrating, over the block of interest, the dot product of the electric fields due to the plane-wave and (fictitious) finite sources. Since the MT impedance is defined in terms of four field components (E_x, E_y, H_x, and H_y), constructing the sensitivity matrix requires forward modeling involving four different finite sources for each measurement site at each frequency. Thus, the total number of forward modelings needed at each inversion iteration is equal to 4×(no. measurement sites)×(no. frequencies). One can see that the computer time can become prohibitive as the numbers of measurement sites and frequencies increase.

A simple way to get around this computational difficulty is to use the sensitivities for a homogeneous half-space in all iterations (Sasaki, 1994; Farquharson and Oldenburg, 1996). Since these sensitivities can be obtained from the analytical solutions of electric fields, they are fast to compute. (Here, this approach is referred to as fast approximate inversion.) However, this method has some limitations in both resolution and convergence as will be shown later. In this study, to obtain a more acceptable result, the following approach is taken: (1) the sensitivities for the starting homogeneous half-space are used in the first few iterations; (2) after that, e.g. at the third iteration, the rigorous sensitivity matrix is generated only once; and (3) in the subsequent iterations, it is updated using Broyden's method (Loke and Barker, 1996; Torres-Verdin *et al.*, 2000).

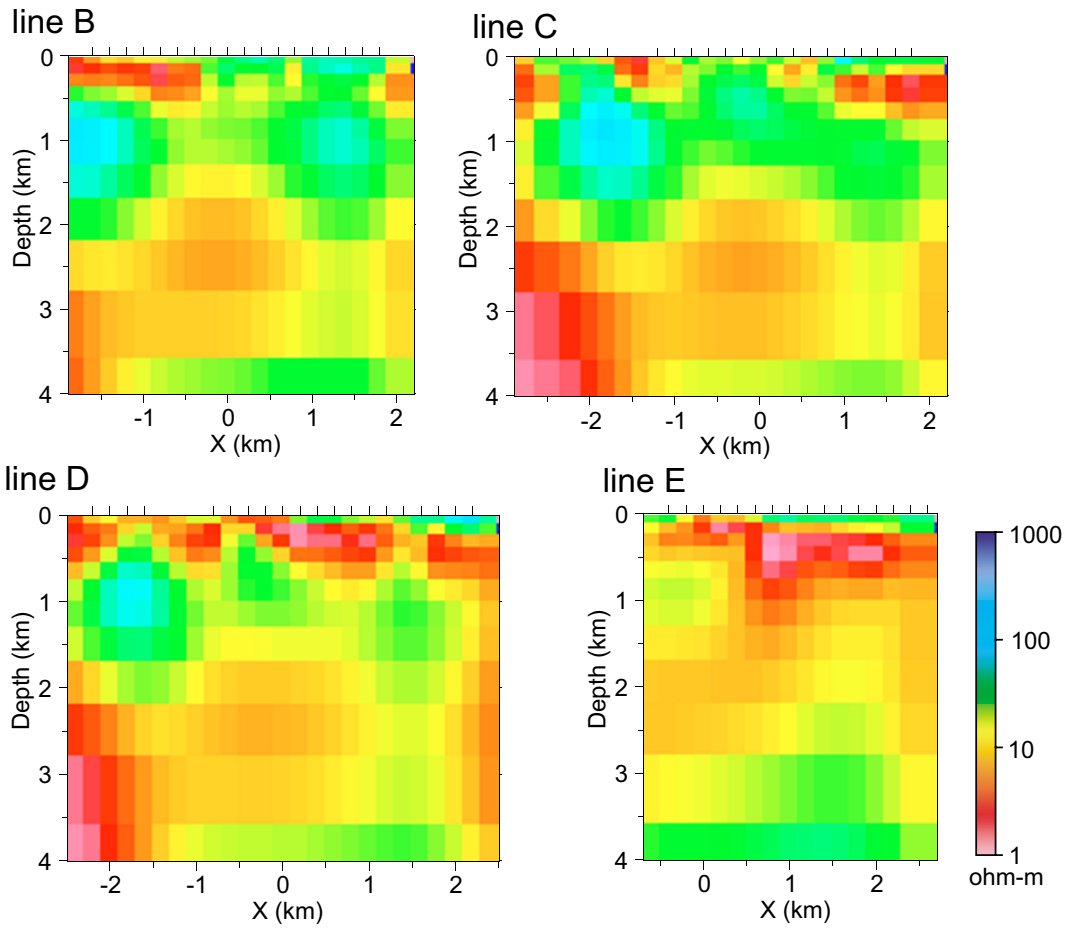

Fig. 10. Vertical sections of the 3-D inversion model along the survey lines B, C, D, and E.

5. Examples

This section presents synthetic and field data examples to illustrate the ability of the inversion algorithm described above in the presence of static shifts as well as to show its performance. All of the results were computed on a 2.53-GHz Pentium 4 PC.

5.1 Synthetic example

The model (Fig. 4) consists of a conductive prism embedded in an otherwise vertical contact media. The prism has dimensions of 400 × 800 × 600 m and its depth of burial is 400 m. The data set was generated using the finite-difference code, over a 10 × 10 grid of 200 m spacing at nine frequencies, ranging from 0.2 to 200 Hz. The data are the apparent resistivities and phases calculated from the off-diagonal elements of the impedance tensor. The total number of real-valued data points is 3600. Prior to inversion, 1.5 percent Gaussian random noise was added to the impedance elements, which translates into standard deviations of 3 percent for the apparent resistivity and 0.9 degrees for the phase. Besides adding the noise, the apparent resistivities were 'static-shifted' using random values from a Gaussian distribution with a mean of zero and a standard deviation of 0.5. Note that static shifts of 0.5 and −0.5 correspond to multiplicative factors of 1.65 ($= e^{0.5}$) and 0.61 ($= e^{-0.5}$), respectively.

In the inversion, the forward modelings were carried out on a 35 × 35 × 29 grid, and the subsurface was divided into 1100 (10 × 10 × 11) blocks. The outer blocks extend to the boundaries of the finite-difference grid, and the inversion domain coincides with the subsurface region of the forward modeling domain. The starting model was a homogeneous half-space of resistivity 30 Ω-m, and the boundary values for this starting model were used as the boundary conditions throughout the iterations. The parameter β was chosen as 0.2; this value is the one among three trial values providing the smallest misfit in the *fast approximate* inversions performed prior to applying the present inversion algorithm. Seven iterations were required to produce the model shown in Fig. 5 and the static shifts in Fig. 6. For comparison, the model obtained from the *fast approximate* inversion is shown in the third column of Fig. 5. The inversion algorithm using the update procedure gives better resolution than that using a constant sensitivity matrix; the vertical contact is better resolved, and the conductive zone left of the contact is also recognizable as an isolated 3-D body. As shown in Fig. 6, the recovered static shifts are in good agreement with the true values. The plots of the data misfit (R) versus iteration number are shown in Fig. 7 for the two cases. It is clear that, as a result of updating sensitivities rigorously at the third iteration, the data misfit converges to the assumed noise level. Incidentally, there was no significant improvement in the convergence when Broyden's method was used throughout the iterations (without calculating the exact sensitivity matrix at the third iteration). This is probably because this quasi-Newton updating method is effective only

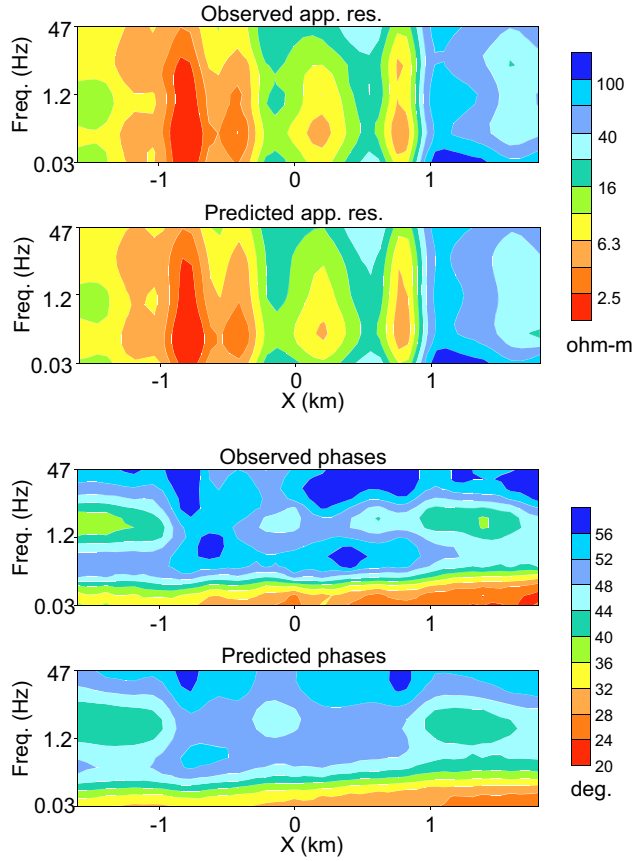

Fig. 11. Comparisons between the observed and predicted xy-mode data along line B. The top two panels are for the apparent resistivities and the bottom two panels are for the phases.

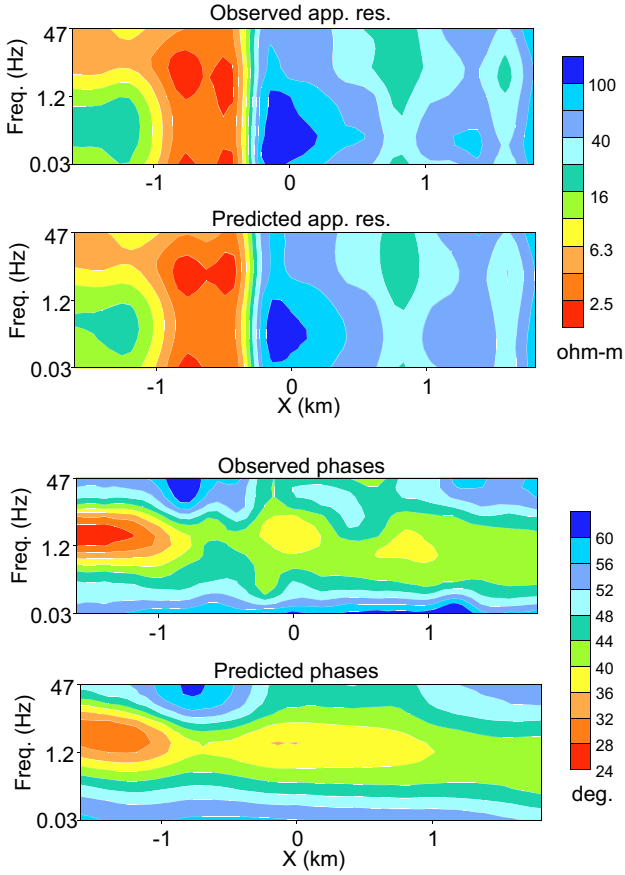

Fig. 12. Comparisons between the observed and predicted yx-mode data along line B.

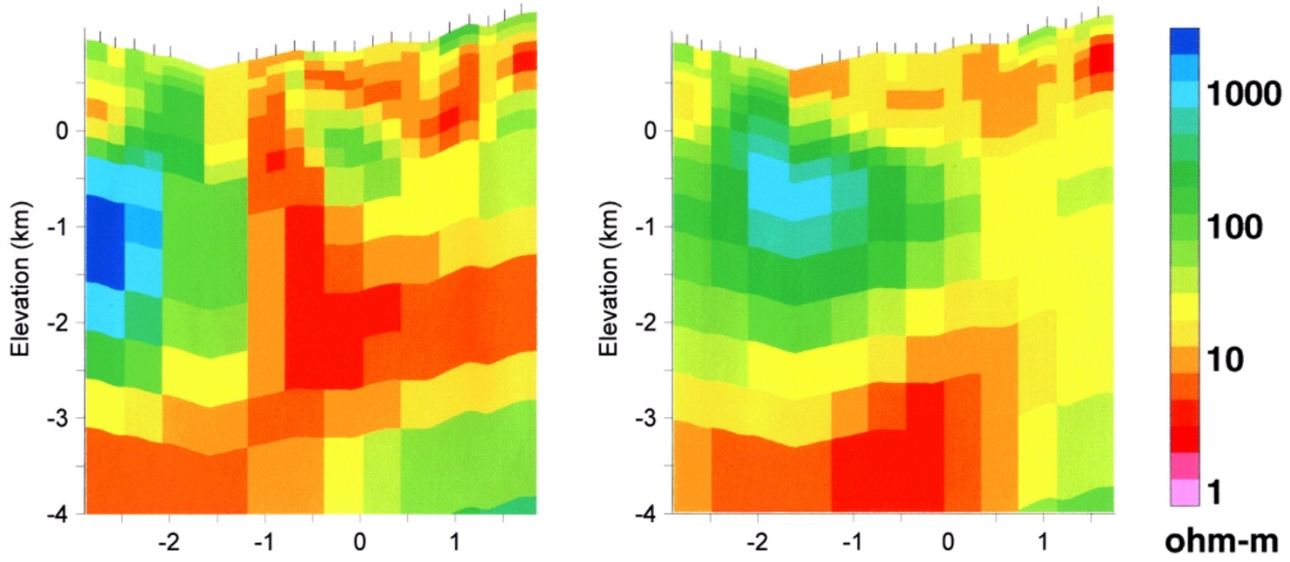

Fig. 13. 2-D inversion results for line C (after Uchida *et al.*, 1999). The left panel is for the TM-mode inversion, and the right panel is for the joint (TM plus TE) mode inversion. The colour scale is different from that of Fig. 10.

if the current estimates are, to some extent, close to the true values. The present inversion procedure required about 7 hr of CPU time. Approximately 6 hr of time was spent on the computation of a full sensitivity matrix involving 3600 additional forward modelings. The *fast approximate* inversion took about 1 hr.

5.2 Field data example

An extensive MT survey was conducted by the New Energy and Industrial Technology Development Organization (NEDO) in 1998 over the Kakkonda geothermal area located in the northern part of Honshu Island, Japan (Uchida *et al.*, 1999). Figure 8 shows the locations of the measurement

sites, which are arranged along four lines B, C, D, and E. These sites are spaced approximately 200 m apart along the lines, except near the power plant, while the line separations are mostly about 600 m. The impedances are rotated to the (x, y) coordinates, where the x axis is nearly along the survey lines. The data set used in the inversion comprises xy and yx mode apparent resistivities and phases at 75 sites and 11 frequencies per site. The frequency range is from 0.03 to 47 Hz. The apparent resistivity and phase curves from line B are shown in Fig. 9. Static-shift effects are obvious in the figure and even more severe than those shown in Jones (1988), indicating complicated near-surface structure.

The inversion model consists of 2704 ($26 \times 8 \times 13$) blocks, and the forward modeling employs a $71 \times 40 \times 32$ grid. The starting model was a homogeneous half-space of 10 Ω-m. The data were assumed to have the same standard deviations. The vertical sections of the inversion model along the four survey lines are shown in Fig. 10, which are obtained with $\beta = 0.8$ after seven iterations. As in the synthetic example, the value of β was chosen among three trial values. The final data misfits are 14.8 percent for the apparent resistivities and 4.2 degrees for the phases. Figures 11 and 12 show the comparisons between the observed and predicted data pseudosection along line B for the xy and yx modes, respectively. They show good agreement, and similar data fits are observed on the other lines. This example required about 24 hr of CPU time and 490 Mbytes of memory.

Overall, the result of the 3-D inversion is consistent with the previous 2-D inversion results (Uchida *et al*., 1999). However, there are some noticeable discrepancies for each line. The resistivity models obtained by 2-D inversions for line C are shown in Fig. 13, where the left panel is from the TM-mode data and the right panel is from the joint (TM plus TE) mode data. In the 2-D inversions, static shifts were not taken into account, although topography was included. It can be seen that the 2-D model from the TM-mode data is closer to the corresponding section of the 3-D model. This is not surprising, because the 2-D inversion of the TE-mode data is more susceptible to both the effects of 3-D structure and static shifts than TM-mode inversion (Wannamaker *et al*., 1984). The main features in the result of 2-D TM-mode inversion are (1) the resistive zone in the south-western part of the 2-D model is located about 1 km deeper than the corresponding zone in the 3-D model, (2) its peak resistivity is much higher (about 3000 vs. 120 Ω-m), and (3) the adjacent conductive zone near a horizontal coordinate $x = -1$ km extends upward. Such features are interpreted to be the distortions caused by the effect of 3-D structure, particularly at depths of less than about 1 km. Note that in Fig. 10, the shallower structure characterized by distinct conductive zones is obviously 3-D, judging from the resistivity variation along the y direction, while the structure at depths of greater than about 1 km is nearly 2-D except in the north-eastern part of line E. In geological circumstances having complex near-surface structure such as geothermal areas, 3-D inversion accounting for static shifts is required even if the regional structure is expected to be 2-D.

6. Conclusions

A robust, efficient method is presented for inverting simultaneously for a 3-D resistivity model and static shifts. As opposed to the previous work on 3-D MT inversion, the method is based on a traditional Gauss-Newton approach that requires a sensitivity calculation. However, the computer time can be greatly reduced by implementing a simple and effective procedure for updating the sensitivity matrix and by using an efficient finite-difference modeling scheme. To stabilize the inversion process, a constraint is imposed so that static shifts are Gaussian distributed with a mean of zero, in addition to a smoothness constraint on the resistivity model. The examples demonstrate that the method is effective in recovering a 3-D resistivity structure from static-shifted data and can be used for 3-D problems of at least moderate size.

Lastly, it must be noted that the diagonal components of the impedance tensor are not used in the 3-D inversions presented here. While some field data examples (Uchida *et al*., 2001; Uchida and Sasaki, 2003) suggest that the dependence of the rotation angle of the coordinate axes on the 3-D inversion result is not significant, it is desirable to invert on the complete impedance tensor, for example, if the rotation angle changes radically with frequency.

Acknowledgments. I thank T. Uchida for his suggestions on the applications of the inversion method to field data sets, which are essential in improving the code. I also thank W. Siripunvaraporn, P. E. Wannamaker, and the editor Y. Ogawa for valuable comments and K. Yamane for making the Kakkonda MT data set available through NEDO. Finally, I am grateful to the Radioactive Waste Management Centre (RWMC) for their permission to publish this paper.

References

deGroot-Hedlin, C., Removal of static shift in two dimensions by regularized inversion, *Geophysics,* **56**, 2102–2106, 1991.

Farquharson, C. G. and D. W. Oldenburg, Approximate sensitivities for the electromagnetic inverse problem, *Geophys. J. Int*., **126**, 235–252, 1996.

Jones, A. G., Static shift of magnetotelluric data and its removal in a sedimentary basin environment, *Geophysics,* **53**, 967–978, 1988.

Loke, M. H. and R. D. Barker, Practical techniques for 3D resistivity surveys and data inversion, *Geophys. Prosp*., **44**, 499–523, 1996.

Mackie, R. L. and T. R. Madden, Three-dimensional magnetotelluric inversion using conjugate gradients, *Geophys. J. Int*., **115**, 215–229, 1993.

Mackie, R. L., T. R. Madden, and P. E. Wannamaker, Three-dimensional magnetotelluric modelling using difference equations: Theory and comparisons to integral equation solutions, *Geophysics,* **58**, 215–226, 1993.

Mackie, R. L., J. T. Smith, and T. R. Madden, Three-dimensional electromagnetic modeling using finite difference equations: The magnetotelluric example, *Radio Sci*., **29**, 923–935, 1994.

Marquardt, D. W., An algorithm for least-squares estimation of nonlinear parameters, *J. Soc. Indust. Appl. Math*., **2**, 431–441, 1963.

McGillivray, P. R., D. W. Oldenburg, R. G. Ellis, and T. M. Habashy, Calculation of sensitivities for the frequency-domain electromagnetic problem, *Geophys. J. Int*., **116**, 1–4, 1994.

Newman, G. A. and D. L. Alumbaugh, Frequency-domain modelling of airborne electromagnetic responses using staggered finite differences, *Geophys. Prospec*., **43**, 1021–1042, 1995.

Newman, G. A. and D. L. Alumbaugh, Three-dimensional magnetotelluric inversion using non-linear conjugate gradients, *Geophys. J. Int*., **140**, 410–424, 2000.

Ogawa, Y. and T. Uchida, A two-dimensional magnetotelluric inversion assuming Gaussian static shift, *Geophys. J. Int*., **126**, 69–76, 1996.

Rodi, W. and R. L. Mackie, Nonlinear conjugate gradients algorithm for 2-D magnetotelluric inversion, *Geophysics,* **66**, 174–187, 2001.

Sasaki, Y., 3-D resistivity inversion using the finite-element method, *Geophysics,* **59**, 1839–1848, 1994.

Siripunvaraporn, W. and G. Egbert, An efficient data-subspace inversion

method for 2-D magnetotelluric data, *Geophysics,* **65**, 791–803, 2000.

Smith, J. T., Conservative modeling of 3-D electromagnetic fields, Part I: properties and error analysis, *Geophysics,* **61**, 1308–1318, 1996a.

Smith, J. T., Conservative modeling of 3-D electromagnetic fields, Part II: Biconjugate gradient solution and an accelerator, *Geophysics,* **61**, 1319–1324, 1996b.

Smith, J. T. and J. R. Booker, Rapid inversion of two- and three-dimensional magnetotelluric data, *J. Geophys. Res.*, **96**, 3905–3922, 1991.

Tarantola, A., *Inverse Problem Theory: Method for Data Fitting and Model Parameter Estimation,* Elsevier, New York, 1987.

Torres-Verdin, C., V. L. Druskin, S. Fang, L. A. Knizhnerman, and A. Malinverno, A dual-grid nonlinear inversion technique with applications to the interpretation of dc resistivity data, *Geophysics,* **65**, 1733–1745, 2000.

Uchida, T. and Y. Sasaki, Stable 3-D inversion of MT data and its application for geothermal exploration, in *Three-Dimensional Electromagnetics III,* edited by J. Macnae and G. Liu, ASEG, **12**, 1–10, 2003.

Uchida, T., Y. Ogawa, S. Takakura, and Y. Mitsuhata, Three-dimensionality of magnetotelluric data in the Kakkonda geothermal field, northern Japan, edited by P. E. Wannamaker and M. S. Zhdanov, Proc. Second Internat. Symposium on Three-dimensional Electromagnetics (3DEM-2), Salt Lake City, 285–288, 1999.

Uchida, T., T. J. Lee, Y. Sasaki, M. Honda, Ashari, and A. Andan, 3-D interpretation of magnetotelluric data at the Bajawa geothermal field, Indonesia, *Geothermal Resources Council Transaction*, **25**, 433–438, 2001.

Wannamaker, P. E., G. W. Hohmann, and S. H. Ward, Magnetotelluric responses of three-dimensional bodies in layered earths, *Geophysics,* **49**, 1517–1533, 1984.

Weidelt, P., Inversion of two-dimensional conductivity structure, *Phys. Earth Planet Inter.*, **10**, 282–291, 1975.

Yamane, K., H. J. Kim, and Y. Ashida, Three-dimensional magnetotelluric inversion using a generalized RRI method and its applications, *Butsuri-Tansa (Geophysical Exploration),* **53**, 234–244, 2000.

Zhdanov, M. S., S. Fang, and G. Hursan, Electromagnetic inversion using quasi-linear approximation, *Geophysics,* **65**, 1501–1513, 2000.

Y. Sasaki (e-mail: sasaki@mine.kyushu-u.ac.jp)